Nucleation of fatigue cracks at the notch tip

LAURA VERGANI, Dipartimento di Meccanica-Politecnico di Milano

Abstract

Notch tip fatigue and fracture behaviour is influenced by local plastic yielding, the extent of which is determined by the notch itself. In this paper, an assessment is made of the influence of the stress-strain gradient on nucleation of notch tip fatigue cracks. The results of a series of experiments performed with a range of theoretical notch factor K_t values are compared with those calculated by applying the Coffin-Manson relation and Neuber's formula.

Riassunto

I processi di fatica e frattura che iniziano da intagli sono influenzati dalla presenza di plasticizzazioni locali la cui estensione è legata all'intaglio stesso.
È stata considerata l'influenza del gradiente degli sforzi e delle deformazioni sulla nucleazione di cricche di fatica da intagli. Sono state condotte numerose prove sperimentali su una gamma di fattori di intaglio teorici Kt.
I valori sperimentali sono stati poi confrontati con quelli calcolati sulla base della legge di Coffin - Manson e della regola di Neuber.

Introduction

Stresses and strains in machine elements often exceed the limit of elasticity of their material owing to notches and/or the fabrication process.

When the operating conditions to which such elements are exposed result in the production of cyclic strains and stresses, areas of high stress concentration become the sites of the nucleation of cracks, whose propagation may result in the failure of a component. Prediction of crack nucleation is thus an essential preventive measure. The Coffin-Manson relation provides a link between total strain and the number of nucleation cycles:

$$\frac{\Delta\varepsilon t}{2} = \frac{\sigma'f}{E} (2N)^b + \varepsilon'f (2N)^c$$

This law, however, is drawn from experiments on cylindrical smooth test specimens with a nil stress gradient (1). In practice, cracks often nucleate from notches, which are the scene of heavy stress concentrations and high gradients. The influence of a notch on the fatigue life of a component cannot by realistically assessed if one ignores the stress-strain field near the crack itself, where the material subjected to less stress and strain supports that subjected to greater stresses (2), (3), (4).

Simplified formulae are usually employed to calculate elastoplastic stresses and strains in the presence of notches. Neuber's rule (5), for example, uses the σ-ε curve of the material to determine the stress-strain value corresponding to the nominal load level. However, this method, too, takes no account of the effect of the stress and strain gradient.

2. Experimental part

2.1 Test specimens

Several sets of "keyhole" specimens with different geometries and hence different theoretical strain concentration factors K_t were constructed (Table 1).

Electric strain gauges were applied to each specimen to show the total and plastic strain patterns on its face and in the crack nucleation zone.

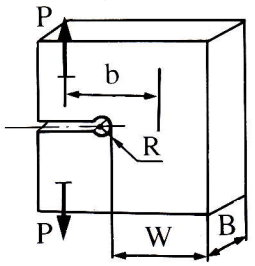

Table 1

Radius R (mm)	B = 24 mm		W = 26,5 mm	B = 17 mm W = 20 mm		
	literature	experimental	numerical	literature	experimental	numerical
2	2,89	2,86	3	2,58	2,56	—
4	2,16	2,3	2,2	—	—	—
12	—	1,48	—	B = 22 mm		W = 27 mm
				—	1,44	1,52

2.2 Material

All the specimens were cut from a 50 mm thick sheet of A 533 grade B steel.

The strength characteristics of this material were determined on other specimens from the same sheet:

R_{el} [N/mm^2]	Rm [N/mm^2]	E [N/mm^2]	ν	A [%]	Z [%]
566	682	210.700	0,28	21	79,8

Its cyclic characteristics were taken from the literature (6):

K ' [N/mm^2]	n '	σ'f [N/mm^2]	ε'f [$\mu \frac{m}{m}$]	b	c
1900	0,183	1137	1199	−0,069	−0,740

2.3 Nucleation tests

A pulsed load was applied with a 250 kN Schenck Hydropulse. Its value was calculated so as to impose the same elastic strain values ($\Delta\varepsilon_{el}$: 5000 μm/m, 5300 μm/m, 5700 μm/m) on each group of specimens, considering that the material behaves elastically.

Nucleation was regarded as present when the crack was revealed by the penetrating liquids.

It was not possible to complete the nucleation test on the Kt = 1.5, B = 24 mm specimens because of high plastic yielding that resulted in their failure at the grip holes.

3. Experimental results

The nominal stress σ_{nom} patterns are plotted against the number of nucleation cycles in Fig. 1. σ_{nom} was calculated by assuming a linear distribution of the stresses in the resistant section:

$$\sigma_{nom} = \frac{P}{BW} + \frac{6Pb}{BW^2}$$

These behaviours illustrate the influence of the K_t value on nucleation.

The strain gauge measurements were used to record the total and plastic strain behaviour of each specimen in function of the number of loading cycles, N.

Fig. 2 shows the total strain $\Delta\varepsilon_t$ patterns in the nucleation zone for specimens with a different Kt, but the same imposed elastic strain value ($\Delta\varepsilon$ 5000 μm/m); while the plastic $\Delta\varepsilon_p$ and residual ε_r strain patterns are illustrated in Figs. 3 e 4 respectively.

The $\Delta\varepsilon_p$ and ε_r strains imposed by the first loading cycle on the entire face of the specimen are illustrated in Fig. 5.

The value of K_t thus has a considerable influence on the behaviour of a specimen. Both $\Delta\varepsilon_p$ and the strain gradients vary in function of K_t, and hence determine the extension of the plastic yield zone.

The pattern displayed by $\Delta\varepsilon_t$ in function of the number of nucleation cycles N_f (Fig. 6) is composed of several curves matching variations in the strain gradient ϱ calculated as the strain variation over 1 mm (see Fig. 5).

Fig. 6 also includes the corresponding values given by the Coffin-Manson law and the characteristics of the material. It can be seen that these values are very conservative. As already stated, this law is founded on tests with cylindrical specimens and hence ϱ = 0. If the gradient is increased, given a certain $\Delta\varepsilon_t$, the number of cycles needed for nucleation, Nf is very much larger.

For example, with cylindrical specimens $\varrho = 0 \frac{\mu m/m}{mm}$, given $\Delta\varepsilon_t = 2500$ μm/m, nucleation takes place after 35.000 cycles, whereas with $\varrho = 2000 \frac{\mu m/m}{mm}$ and the same $\Delta\varepsilon_t$ the nucleation occurs after 50.000 cycles and with $\varrho = 4000 \frac{\mu m/m}{mm}$ Nf = 70.000.

If the total strain values are larger the influence of the gradient is a little lower for example with $\Delta\varepsilon_t = 3000$ μm/m if $\varrho = 0 \frac{\mu m/m}{mm}$ Nf = 15.000, if $\varrho = 2000 \frac{\mu m/m}{mm}$ Nf = 18.000 and if $\varrho = 4.000 \frac{\mu m/m}{mm}$ Nf = 28.000.

When $\Delta\varepsilon_t = 2500$ μm/m passing from $\varrho = 0 \frac{\mu m/m}{mm}$ to $\varrho = 2.000 \frac{\mu m/m}{mm}$ the increase in the nucleation number of cycles is 40%. At $\varrho = 4000 \frac{\mu m/m}{mm}$ the increase is 100%.

When the number of cycles, Nf, is fixed, for example Nf = 20.000, passing from $\varrho = 0 \frac{\mu m/m}{mm}$ to $\varrho = 2000 \frac{\mu m/m}{mm}$ the $\Delta\varepsilon_t$ value is increased of 6%, to $\varrho = 3000 \frac{\mu m/m}{mm}$ the rise is 11% and to $\varrho = 4000 \frac{\mu m/m}{mm}$ is 15%.

It is clear that this can have a considerable influence on the life of a component.

The behaviour of $\Delta\varepsilon_p$ in function of N_f is illustrated in Fig. 7. Since this parameter is an indicator of

the plastic yielding of the specimen and hence of ϱ, it should of greater significance than $\Delta\varepsilon_t$ in the prediction of nucleation. It can be seen, however, that, albeit in a less pronounced manner, the level of $\Delta\varepsilon_p$ is not always uniformly related to N_f, and indication of the extent of the plastic yielding zone is often necessary for correct prediction.

The value of the residual strain ε_r remaining in the specimen after the first loading cycle is heavily influenced by the value of K_t. This is another significant parameter for the prediction of nucleation.

Fig. 8 shows the monotonic σ-ε curve for the material and the first loading cycle for three specimens with different K_t, taken from the strain gauges positioned in the maximum stress zone. It also includes the cyclic curve for the material. After the first loading cycle, the stress becomes virtually alternate with a mean of stress value of about 0. The values of mean ε and (to a lesser extent) mean σ increase near the nucleation zone.

The influence of the gradient cannot be detected when ε_{max} is calculated with Neuber's rule. The governing parameter, in fact, is ε_t, whose levels were made the same for all the sets of specimens. In effect:

$$K_\sigma = \frac{Rel}{\sigma_{nom}} = \frac{Rel}{E\varepsilon_{nom}} = \frac{Rel\ Kt}{E\varepsilon_t} \qquad K_\varepsilon = \frac{\varepsilon_{max}}{\varepsilon_{nom}} = \frac{\varepsilon_{max}\ Kt}{\varepsilon_t}$$

and application of Neuber's rule gives:

$$Kt^2 = K_\sigma\ K_\varepsilon \qquad Kt^2 = \frac{Rel\ Kt}{E\ \varepsilon_t}\ \frac{\varepsilon_{max}\ Kt}{\varepsilon_t}$$

The value of ε_{max} is thus the same for specimens with the same ε_t, but a different K_t.

The experimental values of the maximum strain at the first loading cycle and the theoretical ones, calculated with the Neuber rule, were reported in Table 2.

Table 2

ε_{tot} [μm/m]	ε_{max} [μm/m]								ε_{max} Neuber [μm/m]
	K_t 1,4		2,2		2,6		2,9		
	sp.	num.	sp.	num.	sp.	num.	sp.	num.	
5.700	11.100	11.200	8.200	—	7.600	—	—	8.200	11.900
5.300	9.000	8.200	7.000	7.800	6.500	—	6.900	7.500	10.300
5.000	7.700	8.000	6.400	—	5.600	—	5.700	6.600	9.100

4. Numerical analysis

Numerical models of the test specimens were elaborated with the Abaqus finite elements program (7) (8).

These were all three-dimensional models prepared with 20-node isoparametric elements. Calculations were done in an elastic and elastoplastic field.

The behaviour of the material during the first loading and unloading cycle was reproduced.

There was an excellent fit between the numerical and the experimental results in the elastic field with a maximum error of 5% (Table I), and a good fit in the plastic field (max. error 9%) (Table II).

The numerical and experimental strain behaviour on the face of one specimen is compared in Fig. 9.

5. Conclusions

Our experimental data make it clear that the stress-strain pattern near a notch must be known if one wishes to make a reliable life prediction.

Coffin-Manson's law proved highly conservative when used for this purpose, especially when high gradients are present.

Neuber's rule does not allow the influence of the strain gradient to be determined. In addition, the strain values it gives are too high, with a growing discrepancy with K_t.

The numerical results are in close agreement with the experimental data and enable the strain pattern inside the notch to be determined.

The calculations involved, however, are both complicated and costly. While it is true that they lead to more realistic predictions, it is to be hoped that a simpler approach can be defined.

Acknowledgements

The author wishes to thank M. Giglio for conducting part of the experiments and the numerical calculations.

References

[1] G. Glinka, A. Newport - "Effects of Notch Tip Stress-Strain Calculation Method on the Prediction of Fatigue Crack Initiation Life". 2nd International Conference on Low Cycle Fatigue and Elasto-Plastic Behaviour of Materials - Settembre 87 - Monaco.

[2] A. Esin, B. Uzuner - "A Method to Assess Notched Fatigue Behaviour" Int. J. Fatigue 7 No. (4) 1985 - pp. 215-218.

[3] D. Ellyin "Effect of Tensile-Mean-Strain on Plastic Strain Energy and Cyclic response" J. Engineering Materials and Technology Vol. 107, April (1985), pp. 119-125.

[4] M. Hoffmann, T. Seeger "A generalized Method for Estimating Multiaxial Elastic - Plastic Notch Stresses and Strains" J. Engineering Materials and Technology Vol. 107, October (1985), pp. 250-260.

[5] H. Neuber "Theory of stress Concentration for Shear Strained Prismatical Bodies with Arbitrary Non-linear Stress-Strain Law" Asme Journal of Applied Mechanics, vol. 26, No. 4, 1961, pp. 544-550.

[6] C. Boller, T. Seeger - "Material Data for Cyclic Loading" Material Science Monographs, 42E.

[7] Hibbitt, Karlsson "Abaqus - User's Manual".

[8] M. Giglio "Nucleazione della cricca a fatica in provini intagliati" - Tesi di laurea anno 1986/87 - Politecnico di Milano.

Figure captions

Fig. 1: 1 Nominal stress σ_{nom} in function of the number of nucleation cycles N_f.

Fig. 2: Total strain $\Delta\varepsilon_t$ in function of the number of cycles N in the notch zone for specimens with different K_t, but the same $\Delta\varepsilon_{el} = 5000$.

Fig. 3: Plastic strain $\Delta\varepsilon_p$ in function of the number of cycles N for specimens with different K_t, but the same $\Delta\varepsilon_{el}$.

Fig. 4: Residual strain ε_r in function of the number of cycles N for specimens with different K_t, but the same $\Delta\varepsilon_{el}$.

Fig. 5: Total and residual strains provoked by the first loading cycle on two test specimens with K_t 2.9 and 1.4 respectively, but the same $\Delta\varepsilon_{el} = 5000$.

Fig. 6: Total strain $\Delta\varepsilon_t$ in function of the number of nucleation cycles N_f. The curves vary as the gradient ϱ changes.

Fig. 7: Plastic strain $\Delta\varepsilon_p$ in function of the number of nucleation cycles N_f for two different gradients.

Fig. 8: First loading cycle for test specimens with different K_t. Two cycles in succession are also shown for the specimen with $K_t = 1.4$.

Fig. 9: Experimental and numerical strain patterns produced by the first loading cycle on a specimen with K_t 1.4 and $\Delta\varepsilon_{el}$ 5700.

This work was carried out with the financial support of Ministry of Education 40% grant to Prof. Bernasconi.

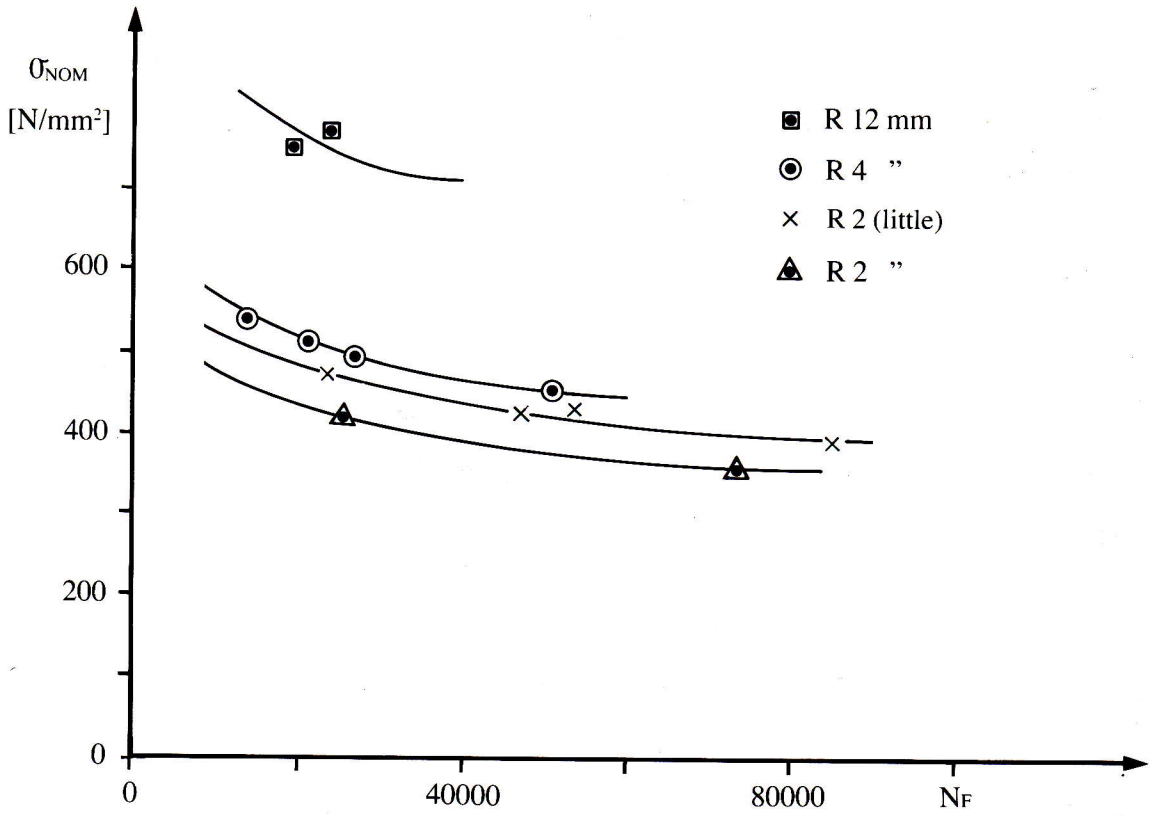
σNOM
[N/mm²]
R 12 mm
R 4 "
R 2 (little)
R 2 "
600
400
200
0
0
40000
80000
NF

Fig. 1

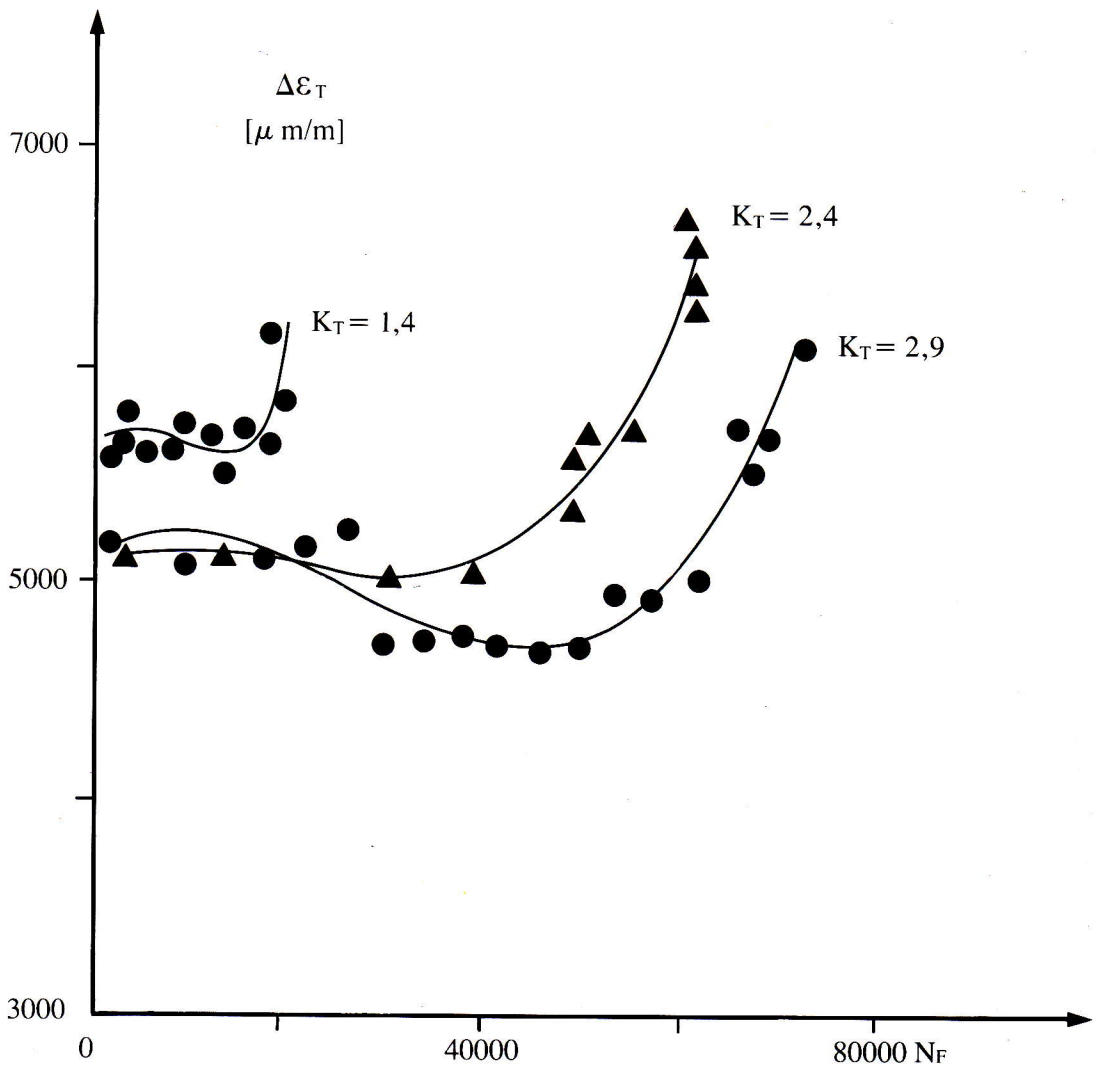
Δε T
[μ m/m]
7000
5000
3000
KT = 2,4
KT = 1,4
KT = 2,9
0
40000
80000 NF

Fig. 2

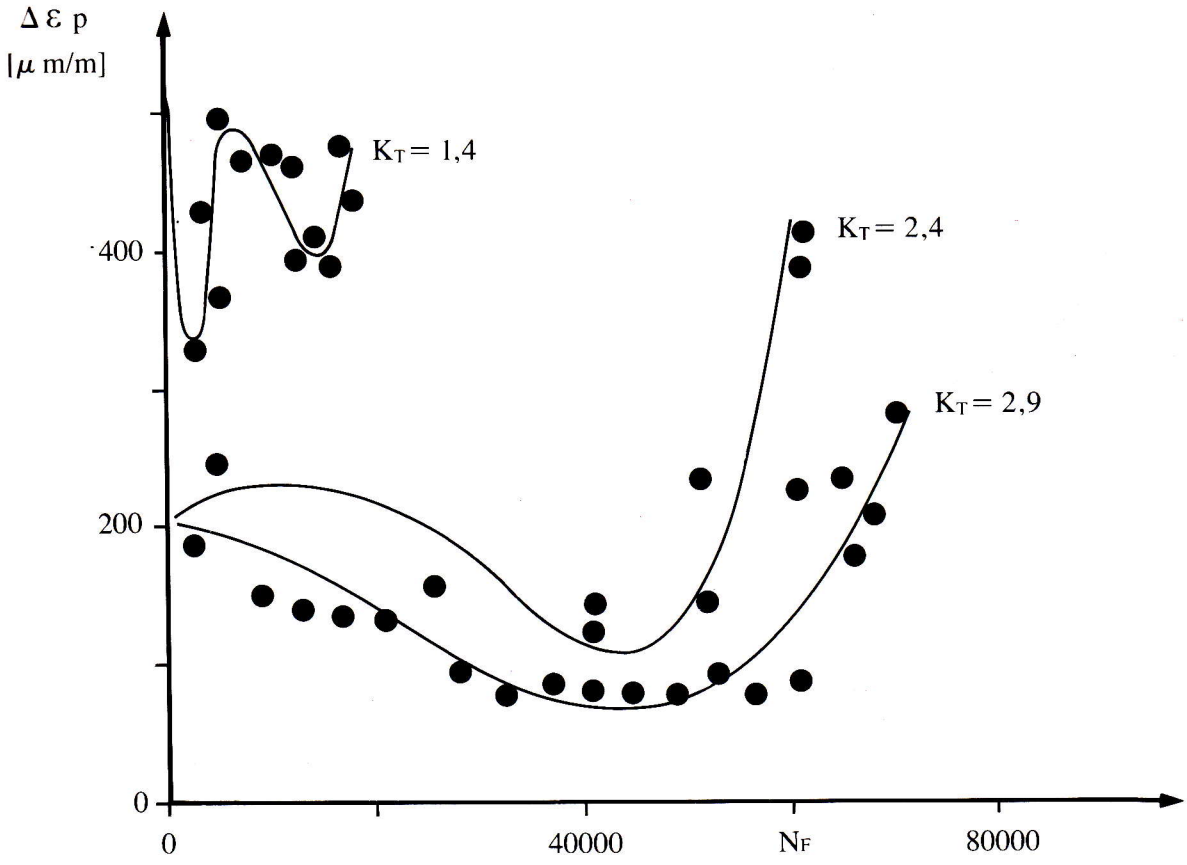
Δ ε p
[μ m/m]
400
200
0
$K_T = 1,4$
$K_T = 2,4$
$K_T = 2,9$
0
40000
N_F
80000

Fig. 3

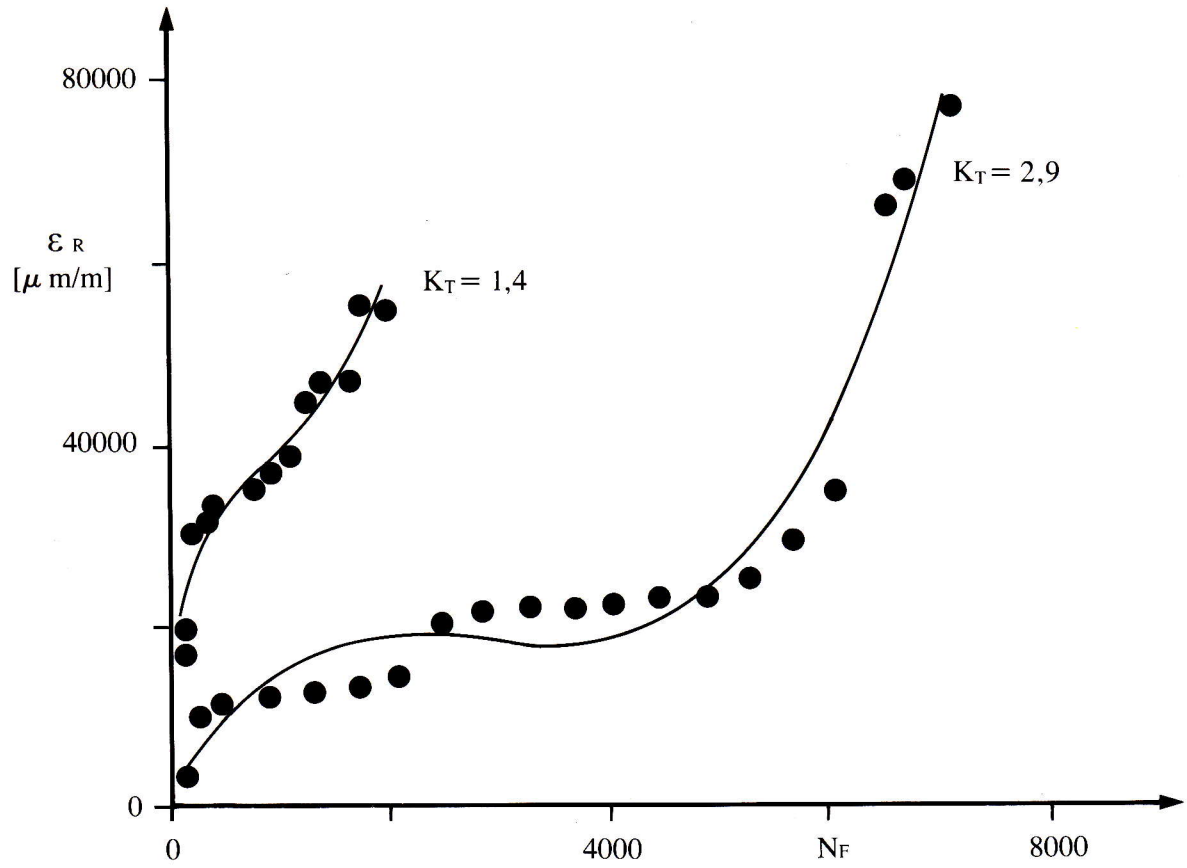
80000
ε R
[μ m/m]
40000
0
$K_T = 2,9$
$K_T = 1,4$
0
4000
N_F
8000

Fig. 4

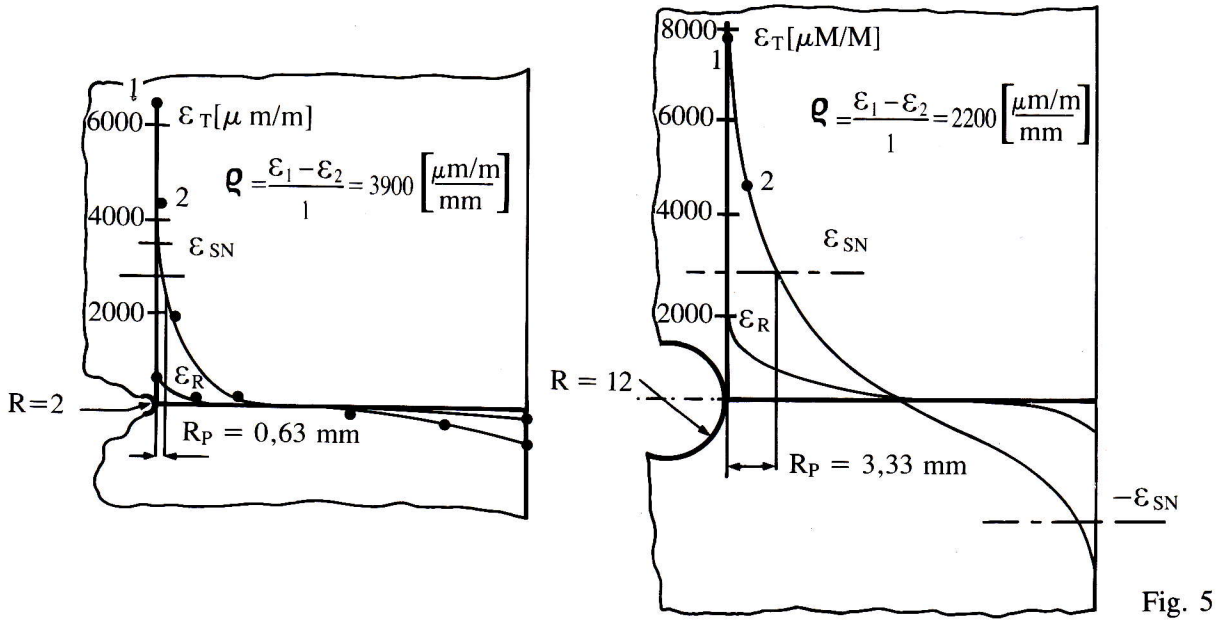
1
6000
$\varepsilon_T[\mu$ m/m]
$\varrho = \frac{\varepsilon_1 - \varepsilon_2}{1} = 3900 \left[\frac{\mu m/m}{mm}\right]$
2
4000
ε_{SN}
2000
ε_R
R=2
R_P = 0,63 mm
8000
$\varepsilon_T[\mu M/M]$
1
6000
$\varrho = \frac{\varepsilon_1 - \varepsilon_2}{1} = 2200 \left[\frac{\mu m/m}{mm}\right]$
2
4000
ε_{SN}
2000
ε_R
R = 12
R_P = 3,33 mm
$-\varepsilon_{SN}$

Fig. 5

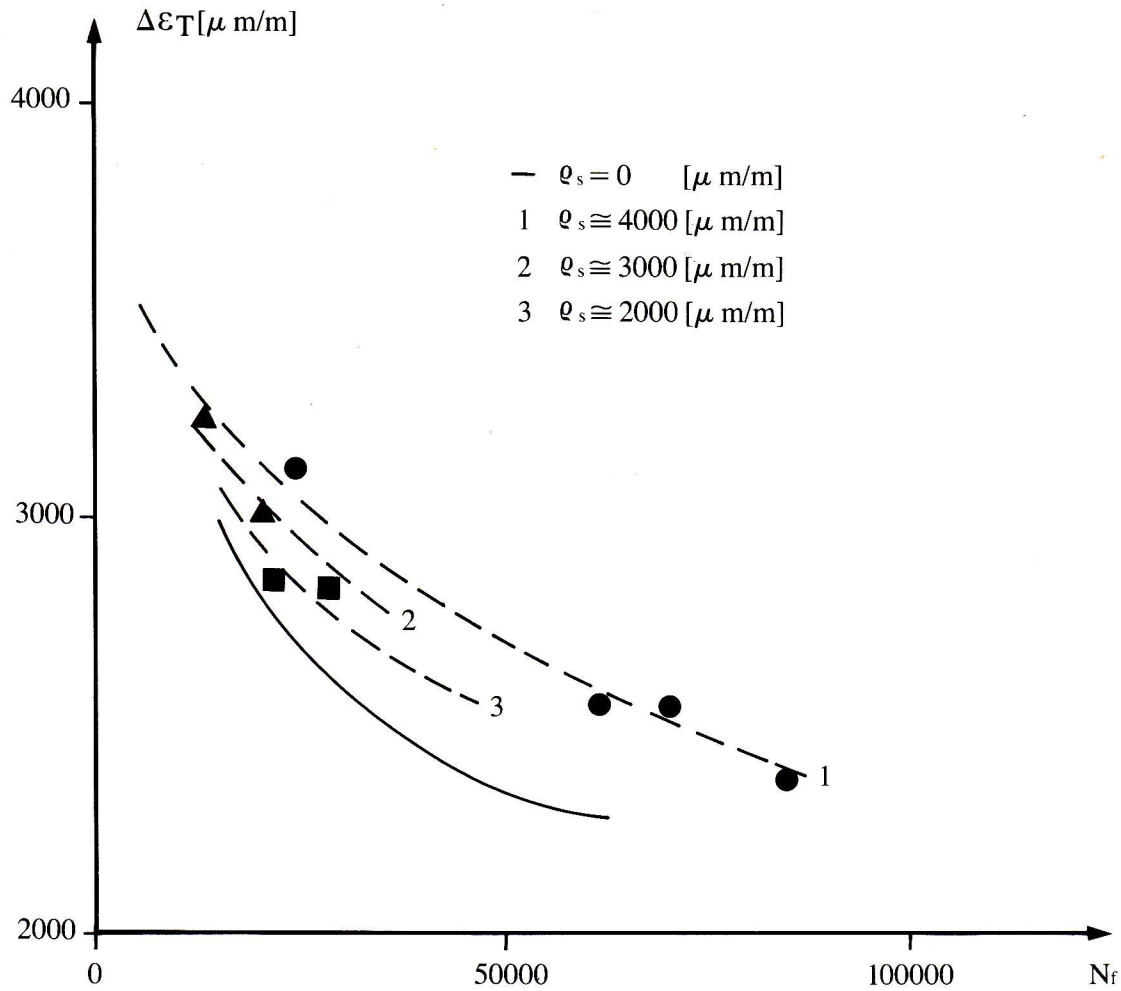
$\Delta\varepsilon_T[\mu$ m/m]
4000
3000
2000
0
50000
100000
N_f
— $\varrho_s = 0$ [μ m/m]
1 $\varrho_s \cong 4000$ [μ m/m]
2 $\varrho_s \cong 3000$ [μ m/m]
3 $\varrho_s \cong 2000$ [μ m/m]
1
2
3

Fig. 6

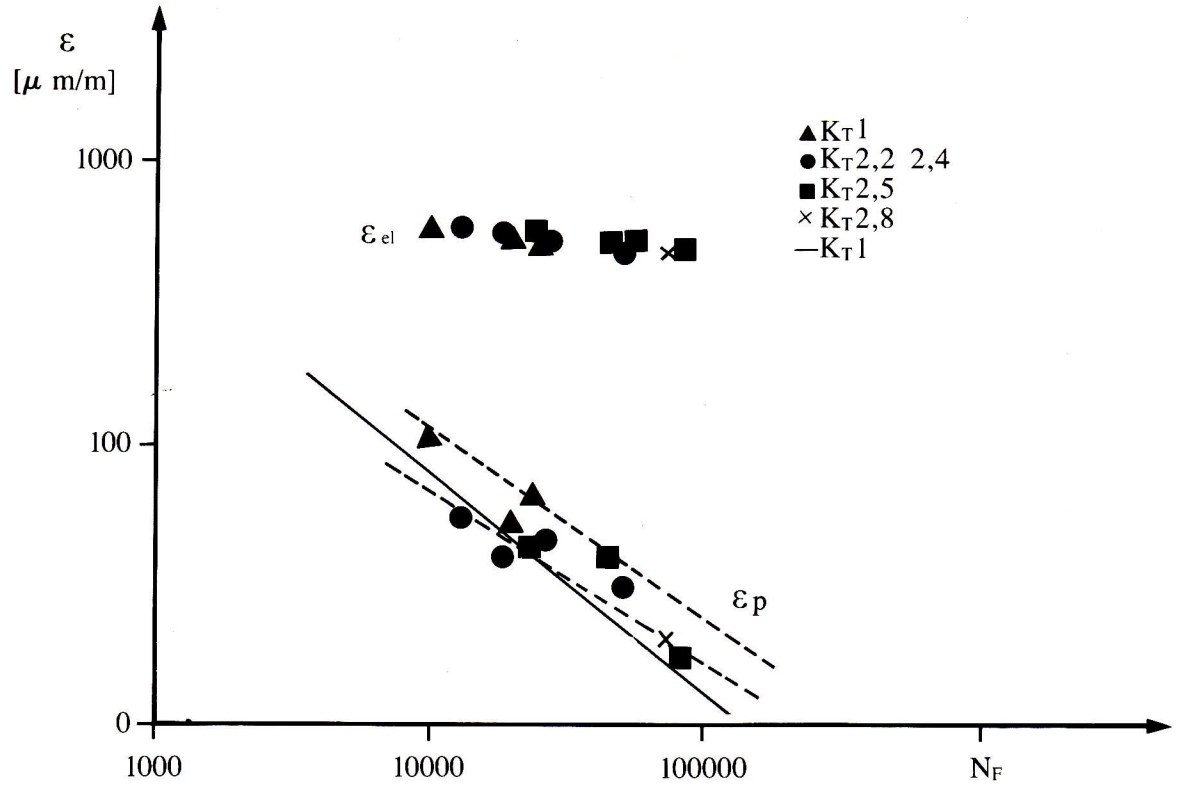
ε
[μ m/m]
1000
100
0
1000
10000
100000
N_F
▲K_T1
●K_T2,2 2,4
■K_T2,5
×K_T2,8
—K_T1
ε_{el}
ε_p

Fig. 7

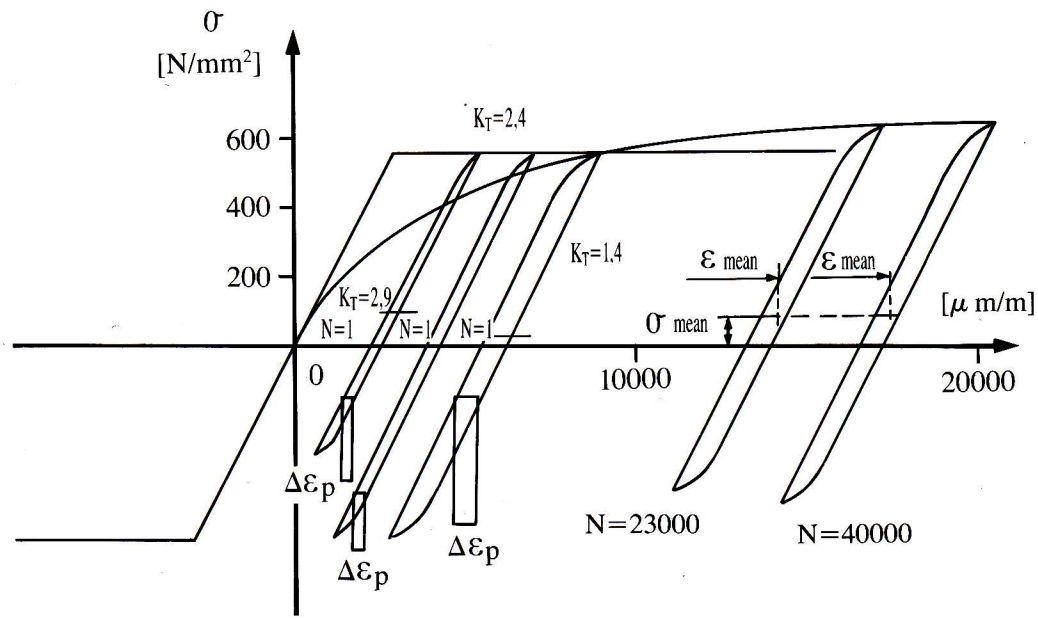
σ
[N/mm²]
600
400
200
0
K_T=2,4
K_T=1,4
K_T=2,9
N=1
N=1
N=1
ε mean
ε mean
σ mean
[μ m/m]
10000
20000
$\Delta\varepsilon_p$
$\Delta\varepsilon_p$
$\Delta\varepsilon_p$
N=23000
N=40000

Fig. 8

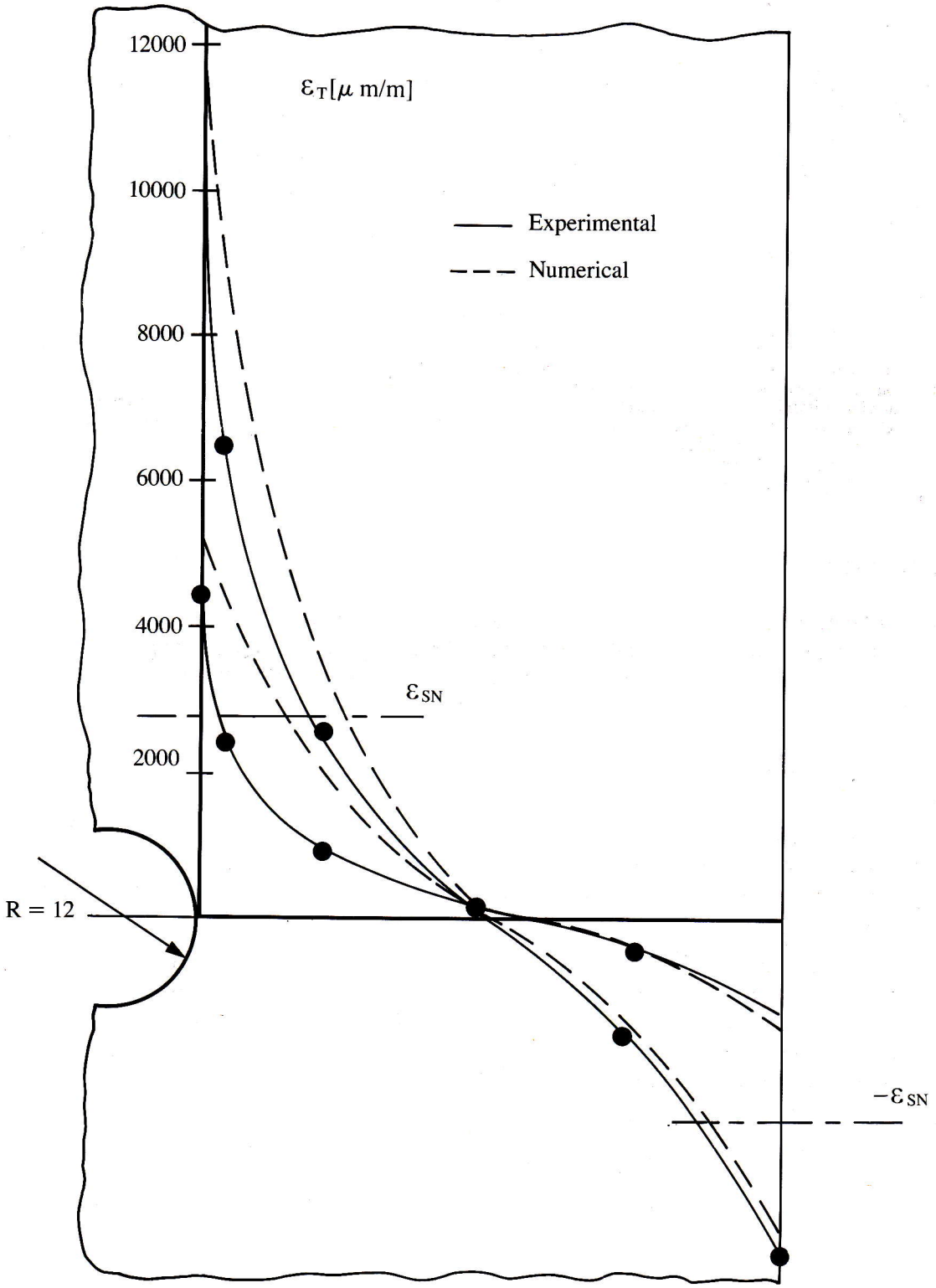
12000
$\varepsilon_T[\mu$ m/m]
10000
Experimental
Numerical
8000
6000
4000
ε_{SN}
2000
R = 12
$-\varepsilon_{SN}$

Fig. 9